Electronic Supplementary Material (ESI) for Soft Matter.

1. SUPPLEMENTARY FIGURES

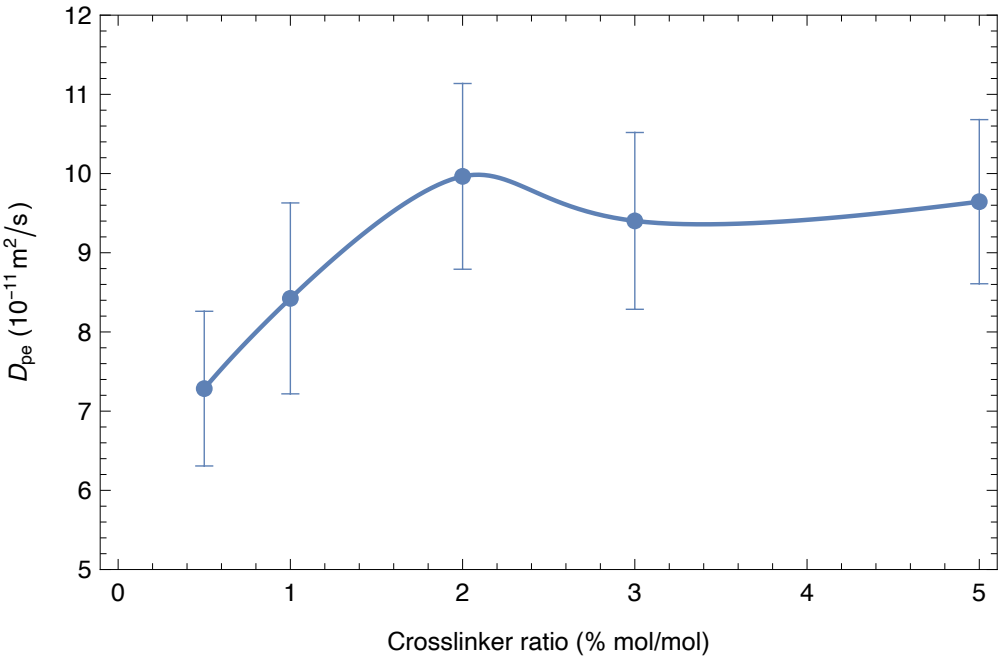

Fig. S1. Poroelastic diffusion coefficient, D_{pe}, of PAAm hydrogels crosslinked with MBA at ratios of 0.5, 1, 2, 3 and 5 (% mol crosslinker/mol monomer). The plot shows that the poroelastic diffusion coefficient is relatively invariant with crosslinking amount.

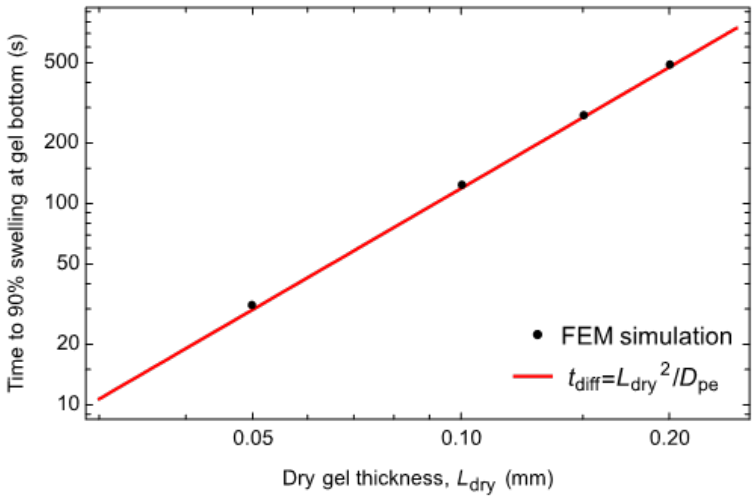

Fig. S2. FEM simulations of the time to 90 % swelling at the bottom of the gel after exposure to a wetted top boundary condition show agreement with the diffusion time scale to within 6%.

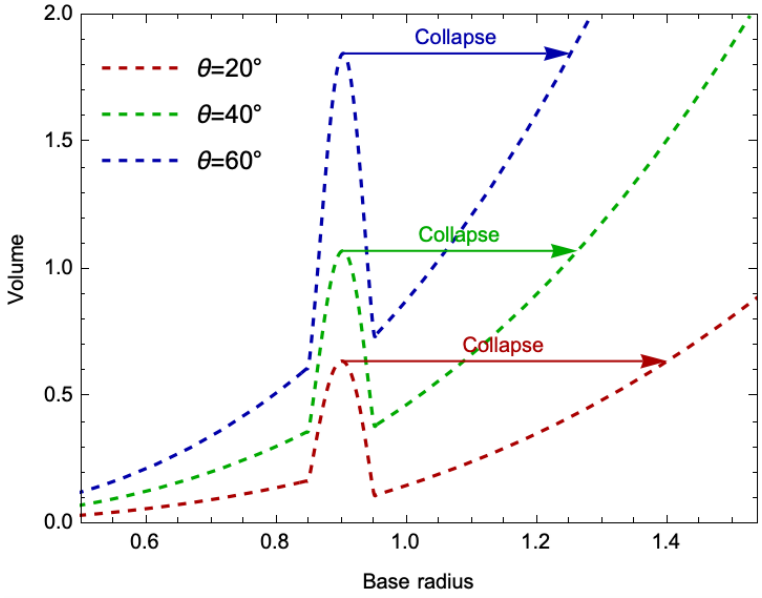

Fig. S3. The relationship between wettability and collapse can be understood from the perspective that collapse is caused by the contact line descending down the slope of the foot. The sloping of the contact angle causes a sudden rise in apparent contact angle and associated volume increase. We have directly calculated spherical droplet volumes as a function of base radius over a foot geometry of varied contact angles to illustrate this point.

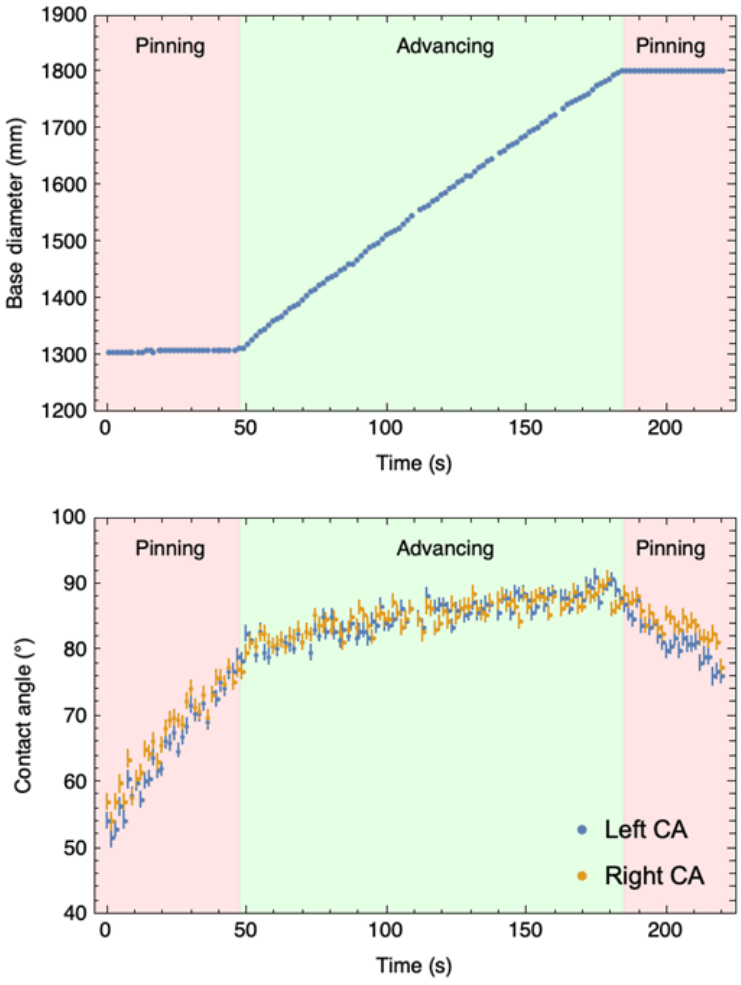

Fig. S4. When an advancing droplet test is performed on a smooth, impermeable substrate (polystyrene), no collapse event was observed, consistent with typical surface behavior.

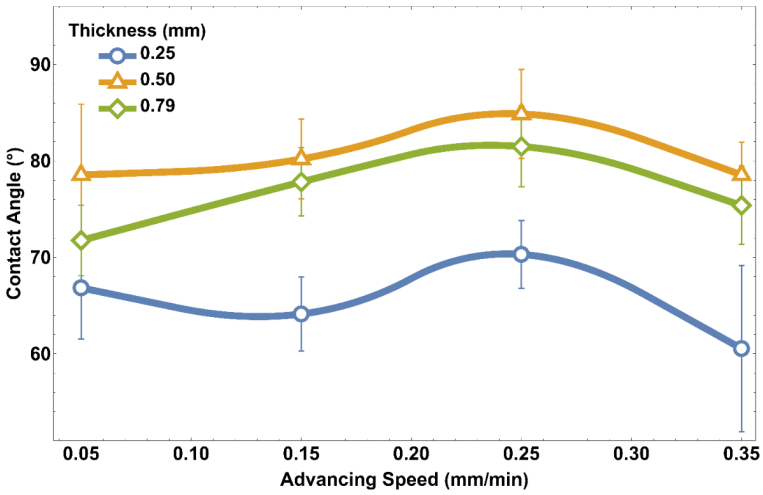

Fig. S5. Measured contact angles for stably advancing droplets on hydrogels of varying thicknesses and advancing speeds. The thinnest samples had slightly reduced contact angles. There is a slight trend of decreased contact angles at higher advancing speeds. Error bars are due to combination of uncertainties arising from differences in left and right angles, uncertainties from the image processing algorithm, and standard deviation errors from sampling multiple frames in the captured videos.

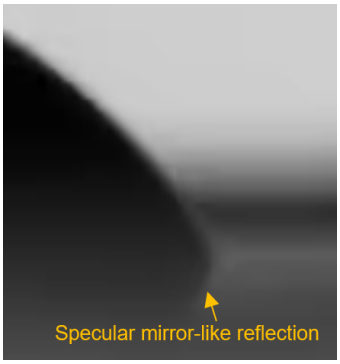

Fig. S6. Mirror-like specular reflections were visible on the surface as shown, indicating that roughness effects were minimal.

2. SUPPLEMENTARY TABLE

Surface Thickness (mm)	Advancing Speed ($mm\,min^{-1}$)	Left Contact Angle (°)	Right Contact Angle (°)	Average Contact Angle (°)
0.79	0.35	$76. \pm 5.$	75.2 ± 3.2	$75. \pm 4.$
0.79	0.25	$79. \pm 13.$	$78 \pm 15.$	$79. \pm 14.$
0.79	0.15	$77. \pm 4.$	78.6 ± 2.7	77.8 ± 3.5
0.79	0.05	$71. \pm 4.$	72.0 ± 3.0	$72. \pm 4.$
0.50	0.35	$79. \pm 4.$	78.4 ± 2.5	78.5 ± 3.4
0.50	0.25	$78. \pm 17.$	$82. \pm 8.$	$80. \pm 13.$
0.50	0.15	$81. \pm 5.$	79.6 ± 3.2	$80. \pm 4.$
0.50	0.05	$79. \pm 9.$	$78. \pm 6.$	$79. \pm 7.$
0.25	0.35	$55. \pm 5.$	65.9 ± 3.1	$61. \pm 9.$
0.25	0.25	$70. \pm 4.$	70.4 ± 2.7	70.3 ± 3.5
0.25	0.15	$64. \pm 5.$	64.1 ± 3.1	$64. \pm 4.$
0.25	0.05	$66. \pm 6.$	$67. \pm 4.$	$67. \pm 5.$

Table S1. The measured advancing contact angles (left, right, and average) of water on top of for 1% crosslinking (mol crosslinker / mol monomer) PAAm hydrogels with thicknesses of 0.25, 0.50, and 0.79 mm. The advancing speed is defined as the change in droplet base radius with time. Advancing speeds were kept below the droplet collapse threshold. The total uncertainty in contact angle measurements are due to a combination of one standard deviation in repeated measurements, fitting uncertainties, and differences between left and right contact angles.

3. SUPPLEMENTARY CALCULATION

Role of droplet shape, its associated capillary pressure, and the effect on chemical potential driving force differences

According to Young-Laplace, we can estimate the capillary pressure change as being on the order of $\sim \gamma/\mathrm{R}$ where γ is the surface tension and R is the droplet radius of curvature. If we imagine a scenario where a contact angle of 0 degrees ($\mathrm{R}\rightarrow\infty$) increases to 90 degrees ($\mathrm{R}=\mathrm{R_{base}}$), this would represent the largest possible capillary pressure difference that could occur, which is on the order of $\Delta p_{\mathrm{cap}} \sim \gamma/\mathrm{R_{base}}$. Using our experimental values, this capillary pressure difference is on the order of $\Delta p_{\mathrm{cap}} \sim 0.10\,\mathrm{Pa}$. Looking gravitational pressure changes due to height changes on the order of 1 mm, $\Delta p_{\mathrm{grav}} \sim \rho g \Delta h \sim 10\,\mathrm{Pa}$. Thus, gravitational effects would be ~ 100 times more important than capillary pressure effects. To understand this pressure difference in the context of chemical potential difference, however, we can evaluate the exact chemical potential difference associated with this gravitational pressure difference, and compare it to the chemical potential difference associated with changes in relative humidity. Defining this ratio as S_{grav} , representing the significance of gravity (numerator) on osmotic driving forces (denominator):

$$\frac{\mu(T_{\mathrm{amb}}, p_{\mathrm{amb}} + \Delta p_{\mathrm{grav}}) - \mu(T_{\mathrm{amb}}, p_{\mathrm{amb}})}{\mu(T_{\mathrm{amb}}, \mathrm{RH} = 100\%) - \mu(T_{\mathrm{amb}}, \mathrm{RH} = 20\%)} = S_{\mathrm{grav}}. \tag{S1}$$

The denominator is equivalent to the chemical potential changes associated with the osmotic driving forces because a "wet", swollen gel is in chemical equilibrium with pure water, which in turn is in chemical equilibrium with pure water vapor (RH=100%), and "dry" gel would be in equilibrium with water vapor at roughly 20% humidity (lab conditions). Osmosis occurs between these "wet" and "dry" states. The numerator of S_{grav} can be calculated directly using IAPWS water properties to be approximately 10 J/mol. The denominator can be calculated using the relation $\mu = \mu_0(T, p) + RTln(\mathrm{RH})$ where $\mu_0(T, p)$ is the chemical potential of pure water vapor. Thus, the denominator is $RT \ln(\frac{100\%}{20\%}) \approx 4000\,\mathrm{J\,mol^{-1}}$ and $S_{\mathrm{grav}} \sim 10^{-3}$. Thus, gravitational pressure contributions to water transport into the gel are three orders of magnitude smaller than osmotic driving forces. Performing the same calculation for capillarity, $S_{\mathrm{cap}} \sim 10^{-5}$; thus, capillary pressure contributions to water transport into the gel are five orders of magnitude smaller than osmotic driving forces. It is reasonable, then, to conclude that gravity and capillarity have negligible effects to the problem at hand.

4. SUPPLEMENTARY VIDEOS

Video S1

A video sped up by a factor of approximately 15x showing the contact angle and base radius changing with time as calculated using image processing. Near the end of the video, the droplet collapses. The gel thickness was 0.50 mm and the advancing speed was 0.35 mm min^{-1}.

Video S2

An animation of a simulated droplet collapse event showing that once the droplet reaches a point on the foot periphery edge corresponding to a local maximum in volume, it must then collapse and jump in base radius, with associated lower apparent contact angle, in order to preserve volume.